Title
Vibrometry as a noncontact alternative to dynamic and viscoelastic mechanical testing in cartilage

Journal
Journal of The Royal Society Interface, 18(185)

ISSN
1742-5689

Authors
Espinosa, M Gabriela
Otarola, Gaston A
Hu, Jerry C
et al.

Publication Date
2021-12-01

DOI
10.1098/rsif.2021.0765

Peer reviewed

INTERFACE

royalsocietypublishing.org/journal/rsif

Research

Cite this article: Espinosa MG, Otarola GA, Hu JC, Athanasiou KA. 2021 Vibrometry as a noncontact alternative to dynamic and viscoelastic mechanical testing in cartilage. *J. R. Soc. Interface* **18**: 20210765. https://doi.org/10.1098/rsif.2021.0765

Received: 3 October 2021
Accepted: 22 November 2021

Subject Category:
Life Sciences–Engineering interface

Subject Areas:
biomedical engineering, biomechanics, bioengineering

Keywords:
vibrometry, dynamic modulus, viscoelasticity, storage modulus, loss modulus, cartilage

Author for correspondence:
Kyriacos A. Athanasiou
e-mail: athens@uci.edu

Electronic supplementary material is available online at https://doi.org/10.6084/m9.figshare.c.5733655.

THE ROYAL SOCIETY PUBLISHING

Vibrometry as a noncontact alternative to dynamic and viscoelastic mechanical testing in cartilage

M. Gabriela Espinosa[1,2], Gaston A. Otarola[1], Jerry C. Hu[1] and Kyriacos A. Athanasiou[1]

[1]Department of Biomedical Engineering, University of California, 3131 Engineering Hall, Irvine, CA 92617, USA
[2]Department of Engineering, Concordia University Irvine, 1530 Concordia West, Irvine, CA 92612, USA

KAA, 0000-0001-5387-8405

Physiological loading of knee cartilage is highly dynamic and may contribute to the progression of osteoarthritis. Thus, an understanding of cartilage's dynamic mechanical properties is crucial in cartilage research. In this study, vibrometry was used as a fast (2 h), noncontact and novel alternative to the slower (30 h), traditional mechanical and biochemical assays for characterization of cartilage from the condyle, patella, trochlear groove and meniscus. Finite-element models predicted tissue resonant frequencies and bending modes, which strongly correlated with experiments ($R^2 = 0.93$). Vibrometry-based viscoelastic properties significantly correlated with moduli from stress relaxation and creep tests, with correlation strengths reaching up to 0.78. Loss modulus also strongly correlated with glycosoaminoglycan (GAG) content. Dynamic properties measured by vibrometry significantly differed among various knee cartilages, ranging between 6.1 and 56.4 MPa. Interestingly, meniscus viscoelastic properties suggest that contrary to common belief, it may lack shock absorption abilities; instead, condylar hyaline cartilage may be a better shock absorber. These data demonstrate for the first time that vibrometry is a noncontact approach to dynamic mechanical characterization of hyaline and fibrocartilage cartilage with concrete relationships to standard quasi-static mechanical testing and biochemical composition. Thus, with a single tool, vibrometry greatly facilitates meeting multiple regulatory recommendations for mechanical characterization of cartilage replacements.

1. Introduction

Cartilage is a dynamically loaded tissue. Typical activities, such as walking, can generate large stresses between 1 and 6 MPa but may even peak up to 12 MPa [1]. These stresses are applied cyclically at frequencies ranging from 0.01 to 2 Hz, typically resulting in up to 4 million loading cycles per year [1,2]. Several factors, such as cyclical mechanical fatigue, excessive strains and rapid strain rates, are often implicated with the onset of osteoarthritis, a condition afflicting approximately 14% of adults [3]. Under cyclical compression, cartilage's biphasic and dynamic mechanical properties protect against these potentially damaging factors via interstitial fluid pressurization [1]. Despite this arguably hostile mechanical environment, cartilage actually relies on cyclic loading for processes such as solute transport and matrix protein synthesis [4]. Given its relevance to daily activities and role in maintaining tissue homeostasis, cartilage dynamic mechanical properties are a crucial component to the field's ongoing research endeavours and to those seeking to replace or regenerate cartilage's function in a dynamic environment.

The importance of cartilage dynamics has not gone unnoted. Cyclic loading has been used to enhance the functional properties of both native and tissue-engineered cartilages [5–7]. Also, for translational purposes, the Food and Drug Administration (FDA) specifically recommends that both static and dynamic mechanical

properties of any knee cartilage repair or replacement product be ascertained [8]. Quasi-static mechanical measurements using viscoelastic testing conditions, such as stress relaxation and creep indentation, are routinely employed to evaluate cartilage and its replacements [9]. Dynamic mechanical testing is often performed under confined compression, unconfined compression or indentation to obtain a dynamic modulus and, occasionally, viscoelastic properties [10,11]. However, most of these mechanical testing modalities are destructive, which either limits the pursuit of certain investigations or requires a large amount of testable tissue. It is certain that a noncontact form of dynamic mechanical testing would garner much attention among cartilage researchers.

Laser Doppler vibrometry has been extensively used in various engineering applications, such as for the assessment of structural stability and rotor vibrations and for the fabrication of micro-electro-mechanical systems devices [12]. One of the first biological applications of vibrometry was in auditory research, specifically measuring vibrations of the tympanic membrane and cochlea [13,14]. Vibrometry has slowly been adopted by others studying biological specimens, such as single cells [15], arteries [16], skin [17] and hydrogels [18]. A major advantage of vibrometry showcased in these works is the ability to perform noncontact and noninvasive measurements. Given this key characteristic, vibrometry is well poised to become a valuable measurement modality in the biological sciences.

The objective of this work was to investigate the use of vibrometry as a noncontact dynamic mechanical testing modality in comparison to quasi-static mechanical and biochemical assays for articular cartilage characterization. Other forms of dynamic testing have shown that dynamic mechanical properties correlate well with quasi-static properties in many biological materials and are typically greater than their quasi-static counterparts [19–22]. This study focuses on the cartilages of the knee, which are known to have differing mechanical properties [23]. We hypothesized that vibrometer-based measurements would recapitulate the relationship between dynamic and quasi-static mechanical properties found through other testing modalities. We further hypothesized that a dynamic structure–function relationship could be ascertained by studying dynamic mechanical properties along with biochemical composition. Lastly, we hypothesized that noncontact laser vibrometry can measure differences in the dynamic modulus and viscoelastic properties of cartilage explants from the condyle, patella, trochlear groove and meniscus. Inclusion of the meniscus, a fibrocartilage, is important for validating vibrometry-based measurements on cartilage tissues with differing mechanical, structural and biochemical properties from hyaline cartilage. The results from this work will enable cartilage researchers to examine native and engineered tissue dynamics without damage, which could facilitate time-course studies surrounding development, disease and repair. These studies may further propel the characterization of cartilage restoration therapies and determine their ability to withstand the dynamic mechanical demands of the native cartilage environment.

2. Methods

2.1. Tissue harvest

Six bovine knee joints from 2- to 4-week-old calves were obtained 48 h post-mortem (Research 87 Inc., Boylston, MA). Using a biopsy punch, 5 mm plugs of cartilaginous tissue were obtained from four different locations: femoral condyle (medial and lateral load-bearing regions), trochlear groove, patella and meniscus (figure 1*a*). All punches were trimmed down to a height of 1.5–2 mm for consistency, maintaining the superficial zone intact and removing the calcified zone. Meniscus punches remained thicker in order to avoid compressive deformation and uneven cutting. The punches were then washed in phosphate buffered saline (PBS) and stored at −20°C. Before testing, all samples were thawed at room temperature in fresh PBS for 1 h. These tissue punches were used for all of the mechanical testing modalities: vibrometry, stress relaxation and creep. The cartilage explants were allowed to recover and equilibrate between tests. It is noteworthy that the geometrical requirements for the samples are imposed by the stress relaxation and creep tests and are not necessary for vibrometry.

2.2. Vibrometry

Tissue deformation due to axial vibrations was measured using a PSV-500-B Xtra Laser Scanning Vibrometer (Polytec). As shown in figure 2*a*, the tissue punch was placed on top of a piezoelectric actuator (P-885.3 PICMA). The punch's bottom surface was secured with wax. The piezo's motion was controlled by the vibrometer's internal function generator. The vibrometer lens was focused on the entire sample surface. Using the high-contrast display option in the PSV 9.4 software (Polytec), a grid with approximately 20 points covering both the sample and piezo was used to align the laser with the live video display. A second higher-density grid (100–150 points) over the same area was then defined to establish the measurement points. It is important to note that measurements were taken of both the sample and the piezo. The function generator was used to generate a chirp signal ranging from 10 to 100 000 Hz to identify resonant frequencies. This was followed by a 500 Hz sinusoidal excitation. Further details on the acquisition settings can be found in electronic supplementary material, table S1. The samples were not damaged and then used to perform destructive mechanical testing.

2.3. Vibrometry analysis

First and second resonant frequencies were found by identifying peaks in the sample velocity data across the frequency sweep (figure 2*b*) using the PSV 9.4 software. For this analysis, data from the piezo were only used to confirm that the piezo's resonant frequencies do not interfere with those of the sample. To differentiate from peaks due to rigid body motion, velocity and deformation were plotted as two-dimensional surfaces to verify the presence of a bending mode at resonance. The dynamic modulus, G^*, of each sample was determined based on the American Society for Testing and Materials International (ASTM International) guidelines for calculating dynamic mechanical properties for disc-shaped specimens via vibration [24,25]. Briefly, for each resonant frequency, a dynamic modulus was calculated,

$$G_i^* = \frac{[37.6991 f_i^2 d^2 m(1-\nu^2)]}{(K_i^2 t^3)}, \tag{2.1}$$

where i is an index referencing either the first or second resonant frequency, f_i are the resonant frequencies, d is the diameter, m is the mass and t is the thickness. Poisson's ratio, ν, is a function of the ratio of the second to first resonant frequencies (f_2/f_1) and the ratio of sample thickness to radius (t/r). In turn, the geometric factors, K_i, are functions of ν and t/r. Functions for ν and K_i were fit to previous empirical data [24,25] using MATLAB (electronic supplementary material, figure S1) and used to

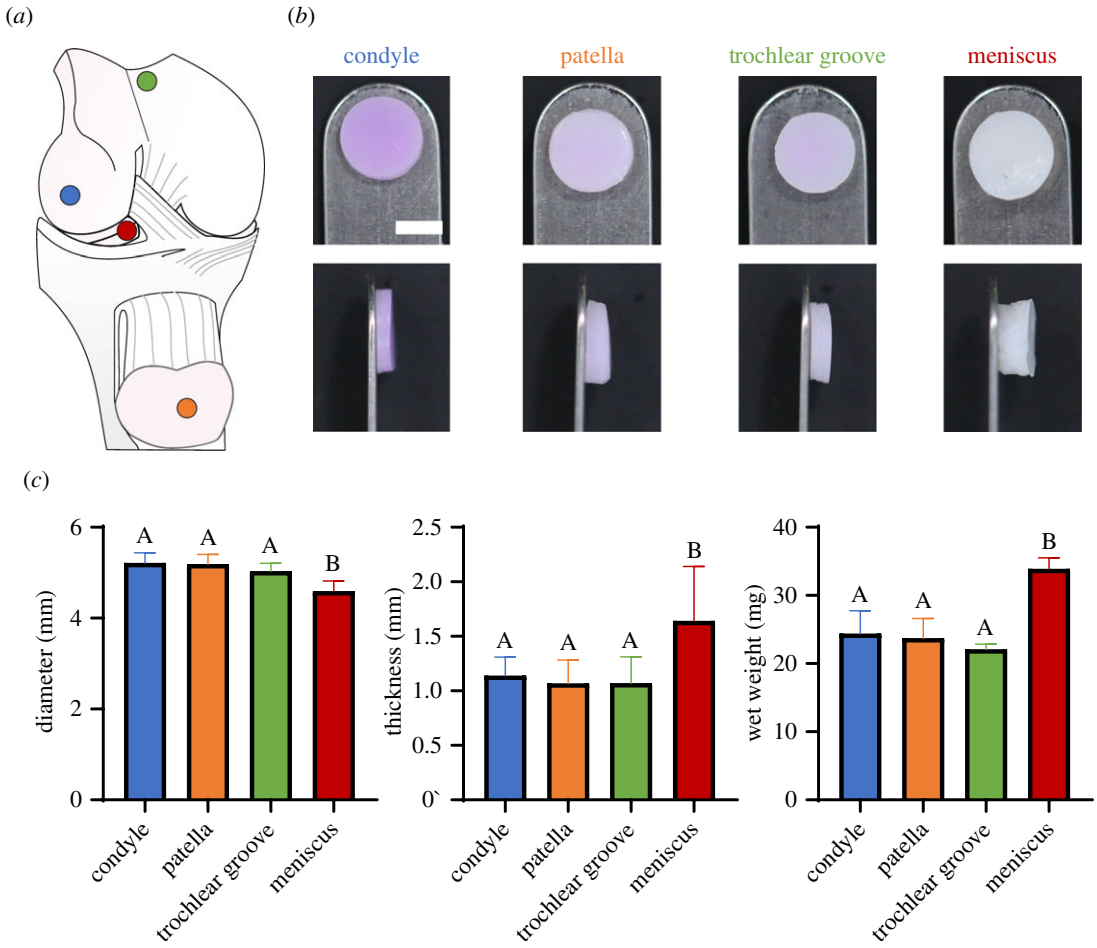

Figure 1. (*a*) Cartilage punches were taken from the condyle (blue), patella (orange), trochlear groove (green) and meniscus (red) of six bovine knee joints. (*b*) Punches were photographed to measure diameter and thickness. Scale bar = 2.5 mm. (*c*) Average diameter, thickness and wet weight for each of the groups. Error bars represent standard deviation and $n = 6$. Groups that do not share the same letter are statistically different.

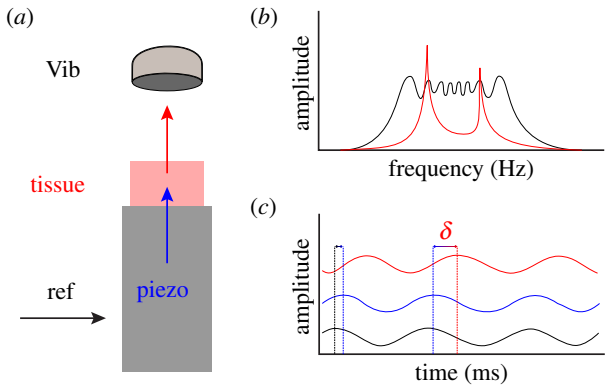

Figure 2. Experimental set-up for vibrometry of cartilage tissue. (*a*) A reference signal (ref) is sent to the piezoelectric actuator, which results in tissue sample deformation. The axial displacement of the tissue's top surface is measured by the vibrometer (Vib). (*b*) A frequency sweep reference signal (black) is used to identify the tissue's resonance peaks (red). (*c*) A sinusoidal reference signal (black) drives the slightly shifted piezo's response (blue). The shift is shown as the difference between the black and blue dotted lines. The tissue's periodic deformation is shown in red, with the phase shift with respect to the piezo signal given by δ.

determine values for the present study. The dynamic moduli for both frequencies were averaged to give a single G^* value per sample.

The viscoelastic properties were determined using the data from sinusoidal excitation (figure 2*c*). Using the PSV 9.4 software, an inverse Fourier transform was used to convert data from the frequency domain to the time domain. In this analysis, data from both the piezo and sample were necessary to measure the phase shift, δ, between the piezo's and tissue's response to the reference signal. The tangent of the phase shift is known to be the ratio of viscous to elastic contributions [26], also known as the loss and storage moduli, respectively. Using G^* and δ, storage and loss moduli were calculated as follows:

$$G' = G^* \cos \delta \tag{2.2a}$$

and

$$G'' = G^* \sin \delta, \tag{2.2b}$$

where G' is the storage modulus and G'' is the loss modulus.

It is important to note that since none of the expressions used to calculate G^*, G' or G'' depends on the displacement or velocity signal amplitudes, there is no need to normalize the tissue response by the piezo data.

2.4. Stress relaxation

Unconfined stress relaxation compressive testing was performed on the 5 mm diameter tissue punches using an Instron model 5565 (Instron, Canton, MA, USA). The samples, which were previously used for nondestructive vibrometry, were placed in a PBS bath at room temperature. Sample heights were determined by lowering a platen that contacts the entire surface until a load change of 0.2 N was detected, and samples were preconditioned at 5% compressive strain for 15 cycles. Stress relaxation tests were performed as follows: samples were compressed to 10% strain at

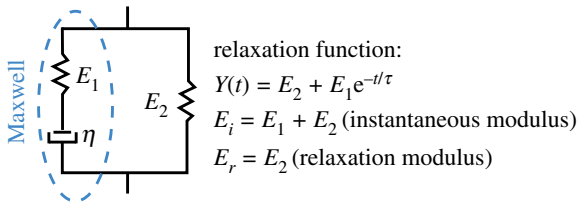

Figure 3. The standard linear solid model consists of a Maxwell component (blue dashed circle) in parallel with a spring. Its relaxation function and definitions for the instantaneous and relaxation moduli are given, where t is time and τ is the relaxation time constant.

a rate of 1% sample height/s, held for 200 s, and then compressed to 20% strain, held for 450 s. The instantaneous modulus (E_i), relaxation modulus (E_r) and coefficient of viscosity of the 10% and 20% strain curves were determined by using the standard linear solid viscoelastic model to fit the data in MATLAB (MathWorks) [27]. The relationships between the instantaneous and relaxation moduli and the component spring elements (E_1 and E_2) are shown in figure 3. The viscoelastic model's springs and dashpot can also be directly related to G' and G'' as shown here:

$$G' = E_2 + \frac{E_1\omega^2}{(E_1^2/\eta^2) + \omega^2} \tag{2.3a}$$

and

$$G'' = \frac{(E_1^2/\eta^2)\omega^2}{(E_1^2/\eta^2) + \omega^2} \tag{2.3b}$$

where ω is the frequency and η is the coefficient of viscosity.

2.5. Creep indentation

A compression indentation apparatus was used to assess creep and recovery deformation of the cartilaginous tissues [28]. Briefly, the 5 mm punches were photographed and glued to a cylindrical sample holder. Indentation was performed using a 1 mm flat-ended, porous indenter tip, perpendicular to the surface at the centre of the sample. The sample surface is assumed to be a semi-infinite half space, which allows the single measurement point to be representative of the whole sample. A 0.5 g tare weight was applied at samples' indentation site, and a variable weight (7.5–10 g for patella and condyle, 4–7.5 g for trochlear and 2–4 g for meniscus) was used to achieve an approximately 10% strain. Sample height was digitally measured using ImageJ (National Institutes of Health).

The aggregate modulus (H_A), shear modulus (μ_s) and permeability were obtained using a semi-analytical, semi-numerical, biphasic model followed by finite-element optimization [29]. The solution process begins with the calculation of μ_s at equilibrium ($t = \infty$) for a specified set of ν values ranging from 0 to 0.499 using

$$\frac{u(\infty)}{h} = \frac{a}{h}\left[\frac{P_0}{2a^2\mu_s}\right]\left[\frac{(1-\nu)}{2\kappa(a/h,\ \nu)}\right], \tag{2.4}$$

where u is the displacement, h is the sample height, a is the radius, P_0 is the load and κ is a function of a/h and ν known as the geometric scaling function [30]. With the exception of ν and κ, all parameters are obtained experimentally. This is followed by the use of a set of specified time (t) values in the expression below:

$$u[\log_{10}(t),\ S]/h = G[\log_{10}(t);\ S,\ P_0/(2\mu_s a^2),\ a/h,\ \nu_s], \tag{2.5a}$$

$$S = \log_{10}(a^2/kH_A) \tag{2.5b}$$

and

$$H_A = 2\mu_s(1-\nu)/(1-2\nu) \tag{2.5c}$$

where S is known as the shift factor, shifting the solution along the logarithmic time axis, and G is the inverse Laplace transform of the creep function. This produces a family of solutions in the (ν, t) plane that can be represented by a bicubic function whose parameters are numerically obtained via curve fitting. This algorithm is described in detail elsewhere [31]. Lastly, these parameters were used as initial guesses for a biphasic model finite-element optimization algorithm that fits the entirety of the creep curve, including the initial rise toward equilibrium [32].

2.6. Validation through finite-element modelling

Abaqus/CAE 2018 (Dassault Systèmes) was used to validate our approach for determining the dynamic modulus of cartilage based on resonance. One representative sample from each group was used to define geometry, mass, G^* and permeability for the models. These values were all directly measured from the methods described above. An encastre boundary condition was imposed on the bottom surface. The models were meshed with 10 344 C3D8R elements. Given the small deformations of the experiment, linear elasticity was assumed. In addition to G^* and permeability, the solid phase of the porous elastic model was also defined by a void ratio, set to 0.5, based on the literature [33,34]. The fluid phase was characterized by the specific weight of the wetting liquid and also based on previous cartilage studies [20,35]. All parameters are listed in electronic supplementary material, table S2. A linear perturbation frequency analysis was performed to find all the resonant frequencies found within 0–20 kHz and their corresponding bending modes. The frequency range was based on the experimental frequency sweeps showing that all first and second resonant frequencies occurred below 20 kHz.

2.7. Biochemical assays

Cartilage tissue samples (approx. 2–3 mg) were weighed before and after lyophilization. The lyophilized samples were digested in 125 µg ml^{-1} papain (Sigma) + 5 mM *N*-acetyl-L-cysteine + (Sigma) 5 mM ethylenediaminetetraacetic acid (EDTA) in phosphate buffer pH 6.5 for 18 h at 60°C. DNA content was measured with a Picogreen assay (ThermoFisher Scientific). Glycosoaminoglycan (GAG) content was measured using a Blyscan glycosaminoglycan assay kit (Biocolor, Newtownabbey, Northern Ireland). Total collagen content was measured using a modified chloramine-T hydroxyproline assay using a bovine Sircol collagen standard (Biocolor) [36]. DNA, GAG and collagen content were measured on a GENios microplate reader (Tecan). For the quantification of pyridinoline (PYR) cross-links, separate tissue samples (approx. 1 mg wet weight (WW)) were weighed, lyophilized and acid digested for 12 h in 6 N HCl. After evaporation, the dried hydrolysate was resuspended in a 75%/25% (v/v) solution of 0.1% formic acid and acetonitrile. Samples were measured through mass spectrometry using a PYR standard (BOC Sciences) and a Cogent diamond hydride 2.0 HPLC column (Avantor, VWR) with a flow rate of 400 µl min^{-1} on an ACQUITY UPLC I-Class core system with an ACQUITY Qda quadrupole mass spectrometer (Waters) [37].

2.8. Statistics and accessibility

All data are reported as average ± standard deviation. Two-way and one-way analysis of variances (ANOVAs) with Tukey's *post-hoc* test (GraphPad Prism 8.1.1) were used to determine statistical significance. Measured and modelled resonant frequencies were found to be normally distributed and were correlated using the Pearson correlation test. Correlations between dynamic vibrometer measures and quasi-static and biochemical measures were performed using the Spearman's ρ-test. Correlation strengths, ρ, are generally considered strong if greater than or equal to 0.70, moderate if between 0.40 and 0.69 and weak if less than 0.40 [38]. This study's datasets can be found on the Dryad Digital Repository [39].

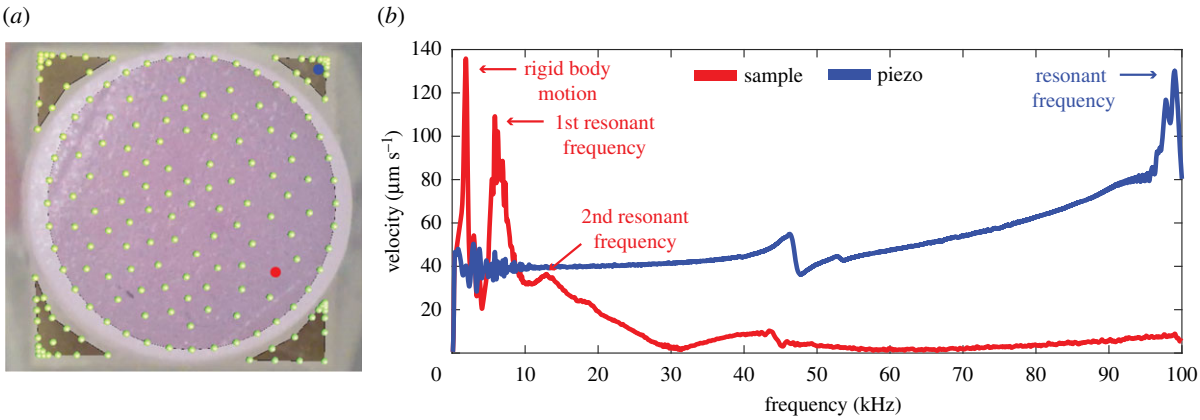

Figure 4. Green points show measurement locations throughout both the sample and the piezo (*a*). Frequency spectra from the red and blue dots are shown in (*b*), with rigid body motion and resonant peaks labelled.

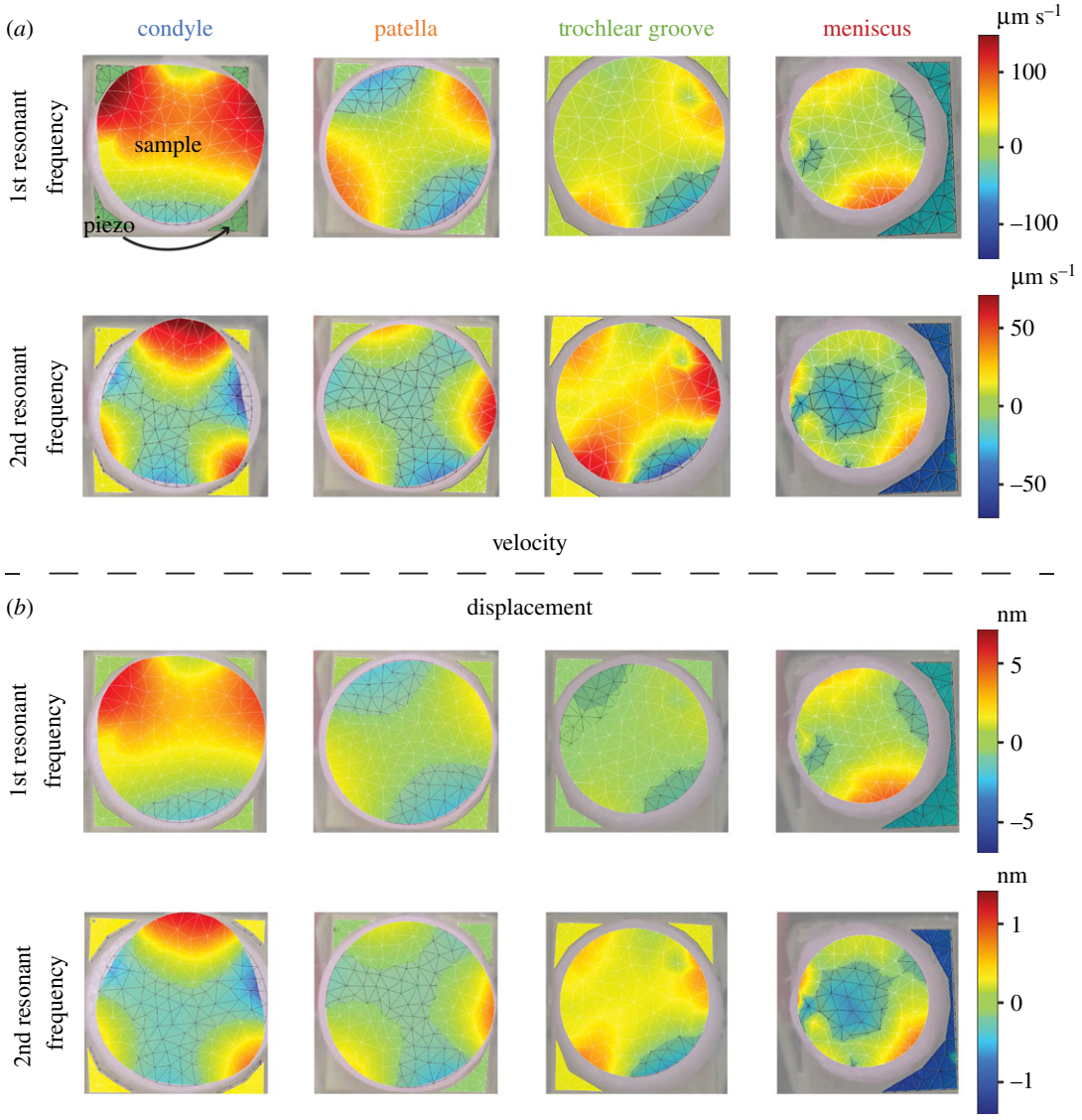

Figure 5. (*a*) Representative images of velocity plotted over the tissue and underlying piezo platform (arrow). (*b*) Tissue displacements demonstrate the bending modes for samples from each group at their respective first and second resonant frequencies.

3. Results

3.1. Tissue sample physical properties

Tissue punches were obtained from the condyle, patella, trochlear groove and meniscus. Although the punches from the other groups were consistent in size, meniscus punches had a significantly smaller diameter (figure 1*c*). Compared to the condyle, patella and trochlear groove, meniscus explant diameters were 11.9%, 11.5% and 8.7% smaller, respectively. The meniscus punches also had a significantly greater thickness and WW compared to all other groups. The meniscus samples showed a 44.2%, 53.8% and 53.4% increased

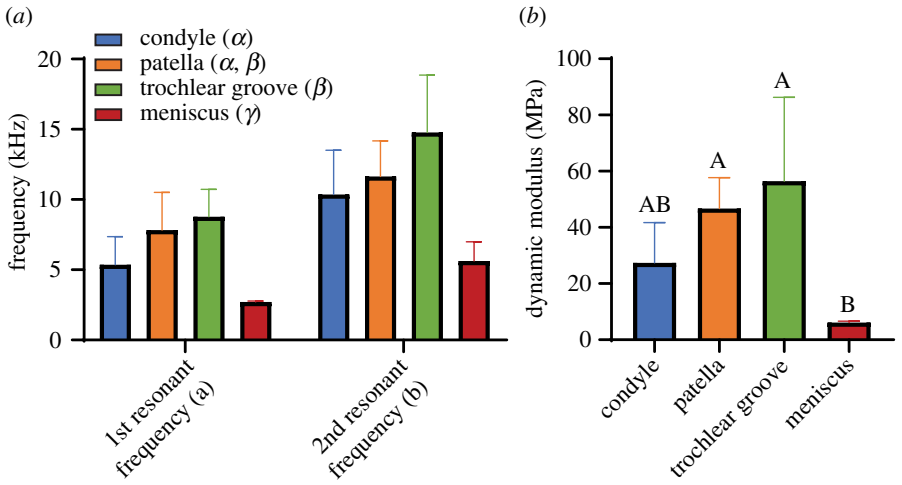

Figure 6. (*a*) Average first and second resonant frequencies significantly differ among the cartilages of the knee. A two-way ANOVA is presented with the factors of frequency (lower case Latin characters) and cartilage group (Greek characters). Both factors were significant. Letters not shared between groups within a factor denote significant differences. (*b*) The dynamic moduli are determined from the resonant frequencies and follow a similar trend. Capitalized letters not shared between groups denote significant differences by a one-way ANOVA. For all data, error bars show the positive standard deviation and $n = 6$.

thickness and 39.0%, 43.0% and 53.4% increased WW when compared to the condyle, patella and trochlear groove, respectively. Dimensional and weight data were used to normalize data and obtain mechanical properties.

3.2. Vibrometry

Vibrational spectra were obtained for measurement points on the sample and piezo, as depicted in figure 4*a*. Representative data are shown in figure 4*b*. In order to distinguish between rigid body motion and resonance, bending mode shapes were identified for each group's first and second resonant frequencies (figure 5 and electronic supplementary material, videos S1 and S2). Mode shapes are often described by nodal lines or circles (electronic supplementary material, figure S2) [40]. For example, a mode with one nodal line, but no circles, is denoted by (0, 1). Points along nodal lines and circles are relatively stable at resonance compared to other areas. The first resonant frequency's bending mode, (0, 2), was characterized by displacements that were symmetrical around two orthogonal nodal diameters in-plane with the sample, and was known as a saddle mode [24]. This shape was consistent across all groups. The second resonant frequency for the condyle, patella and trochlear groove was characterized by symmetry around three nodal diameters, (0, 3). The second resonant frequency for the meniscus differed from the rest, consisting of a single nodal circle, (1, 0). This mode is often referred to as a breathing mode. Videos of the bending modes at resonance can be found in the electronic supplementary material.

3.2.1. Resonant frequencies and dynamic moduli

First resonant frequencies for the condyle, patella and trochlear groove were 5352 ± 2011 Hz, 7823 ± 2682 Hz and 8768 ± 1957 Hz, respectively (figure 6*a*). An increasing trend was observed, with the trochlear groove being significantly greater than the condyle. The first resonant frequency for the meniscus was 2708 ± 65 Hz, significantly lower than all the other groups. The trends observed with the first resonant frequencies were repeated with the second resonant frequencies. Figure 6*b* shows the dynamic moduli, calculated based on resonant frequencies. The relationship among the groups was maintained. Dynamic moduli were 27.4 ± 14.3 MPa, 46.7 ± 11.0 MPa, 56.4 ± 29.9 and 6.1 ± 0.5 MPa for the condyle, patella, trochlear groove and meniscus, respectively.

3.2.2. Viscoelastic properties

In addition to the significant differences in dynamic modulus, there were also considerable differences among the groups' phase shifts, δ. The measured phase shifts were $7.0 \pm 1.4°$, $3.8 \pm 2.0°$, $2.1 \pm 1.0°$ and $8.2 \pm 0.2°$ for the condyle, patella, trochlear groove and meniscus, respectively (figure 7*a*). The tangents of the phase shifts for the patella and trochlear groove were 46% and 70% lower compared to the condyle, respectively. Although this did not result in significant differences in G' among these three groups (figure 7*b*), the differences in their G'' did reach statistical significance. The loss moduli (figure 7*c*) for the condyle, patella and trochlear groove were 4.0 ± 0.3 MPa, 3.1 ± 1.6 MPa and 1.6 ± 0.2 MPa, respectively. The meniscus followed a different pattern from the hyaline cartilage groups ($G'' = 0.9 \pm 0.1$ MPa). Although the tangent of the phase was comparable to the condyle's, the meniscus had a substantially lower G' and G'' compared to the condyle, reaching statistical significance in the case of the loss modulus.

3.3. Quasi-static mechanics

Representative curves and model fits for stress relaxation and creep tests are shown in figure 8. Stress relaxation was performed at 10% and 20% strain. There were no statistically significant differences among the groups for either instantaneous modulus (figure 9*a*) or viscosity (not shown) at either strain. The relaxation modulus (figure 9*b*) for the meniscus at 20% strain was significantly lower than the condyle's by 83%. Both aggregate and shear moduli (figure 9*c*) from creep indentation tests were significantly different among the groups. For example, the trochlear groove and meniscus aggregate moduli were reduced by 44% and 87% compared to the

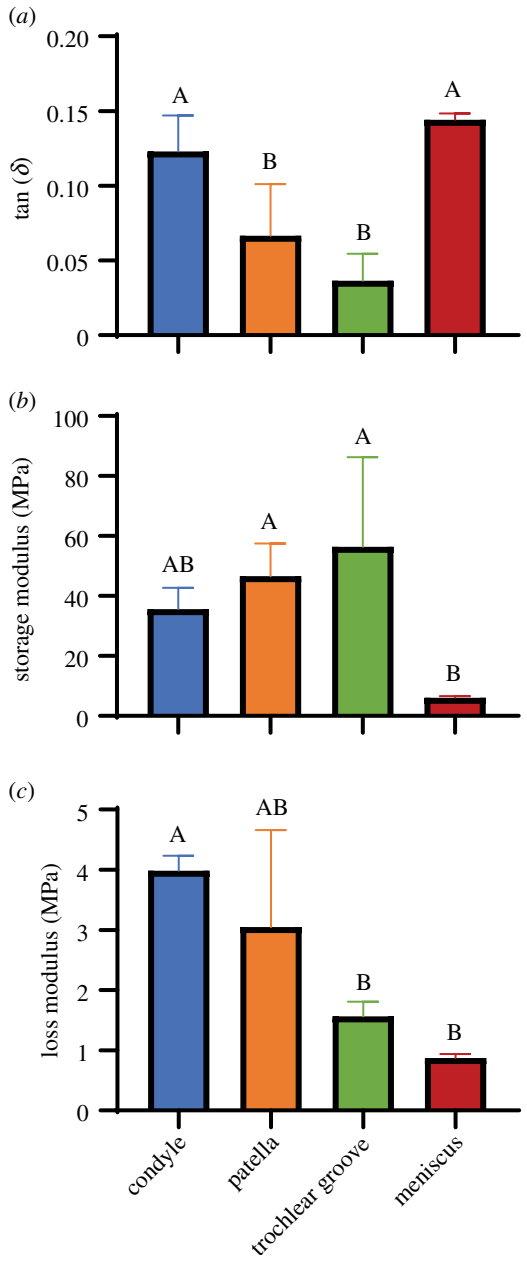

Figure 7. Phase shifts (δ) were measured to determine viscoelastic properties. (*a*) The tangent of δ represents the ratio of viscous to elastic contributions to the tissue's mechanics. This is significantly greater for the condyle and meniscus than the patella and trochlear groove. The storage (*b*) and loss (*c*) moduli trend differently, but in both cases, the meniscus has the lowest values. Error bars represent standard deviation and $n = 6$.

condyle, respectively. Several quasi-static measures followed similar trends to those obtained through vibrometry. Instantaneous modulus correlated with G', while relaxation, aggregate and shear moduli correlated with G''.

3.4. Finite-element validation

The experimental (figure 5) and computationally predicted (figure 10*a*) bending modes were strikingly similar for the condyle, patella and trochlear groove. The predicted displacements for the meniscus were small and thus scaled differently (figure 10*a*–insets). For the meniscus, the predicted first and second resonant frequency modes were characterized by one and four nodal diameters, respectively. Taken together, the measured and modelled resonant frequencies significantly and strongly correlated across all tissues ($R^2 = 0.93$, figure 10*b*) with a slope of approximately 1, providing strong validation of the experimental approach.

3.5. Biochemical composition

Hydration of the tissue samples was relatively similar among the condyle, patella and trochlear groove, averaging around 79% (figure 11*a*). The meniscus was significantly less hydrated at 71 ± 4%. With regards to collagen/WW (figure 11*b*), the condyle's collagen content was significantly lower than all other groups at only 7.6 ± 0.6%. The patella (12.9 ± 2.3%) and trochlear groove (11.6 ± 0.8%) were not statistically different from each other, but both had significantly less collagen than the meniscus (24.6 ± 3.7%). The meniscus had over three times more collagen content than was present in the condyle. PYR/WW (figure 11*c*) followed the same trend as collagen: 916.1 ± 48.2 ng mg^{-1}, 1363 ± 217.3 ng mg^{-1}, 1208 ± 233.0 ng mg^{-1} and 3355 ± 697.0 ng mg^{-1} for the condyle, patella, trochlear groove and meniscus, respectively. The inverse trend was observed with GAG content (figure 11*d*). The condyle's GAG content (4.8 ± 0.5%) was more than eight times that found in the meniscus (0.6 ± 0.2%). The GAG content found in the patella and trochlear groove was 2.6 ± 1.1% and 2.7 ± 0.9%, respectively.

3.6. Comparison between measurement techniques

Several correlations between dynamic mechanical properties and quasi-static properties and between dynamic mechanical properties and biochemical composition were found (figure 12). The dynamic modulus, G^*, was most strongly and significantly correlated with the 10% and 20% instantaneous moduli from stress relaxation ($\rho \geq 0.65$, $p = 0.001$). No associations were found between G^* and creep indentation parameters or between G^* and biochemical components. The storage modulus, G', which was proportional to G^*, was solely correlated to the instantaneous moduli. The loss modulus, G'', trended with the relaxation moduli, reaching statistical significance with the values from the 20% strain stress relaxation tests. G'' was more strongly related to the properties obtained from creep indentation. For example, the correlation between G'' and shear modulus had a strength of 0.78 ($p = 0.002$). Similarly, G'' was also strongly correlated with GAG content ($\rho = 0.72$, $p = 0.002$).

4. Discussion

Physiological loading of knee articular cartilage is highly dynamic. This loading environment is necessary for nutrient transport and mechanical signalling [4], but may also result in tissue fatigue and the eventual onset of osteoarthritis [3]. Therefore, as recommended by the FDA [8], mechanical characterization of cartilage replacements should include both static and dynamic testing. Most dynamic tests used in cartilage research are destructive, often limiting the scope of a study due to tissue scarcity. Given the success of vibrometry in engineering and even a few biological applications, this study's objective was to investigate the use of vibrometry as a noncontact method for dynamic mechanical testing of cartilage. Our first hypothesis was that dynamic measurements from vibrometry would correlate with those obtained from quasi-static mechanical testing, as shown in previous studies using other dynamic mechanical testing modalities [20]. The second hypothesis was that vibrometry and

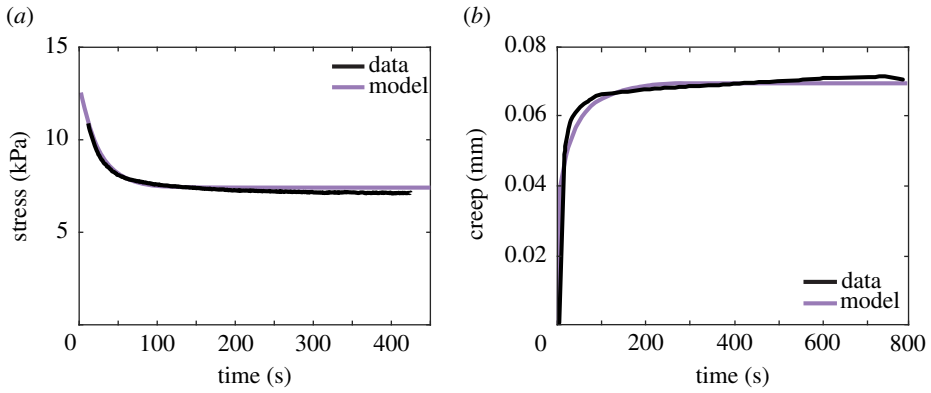

Figure 8. Representative data (black) and model fits (purple) for stress relaxation (*a*) and creep (*b*) experiments.

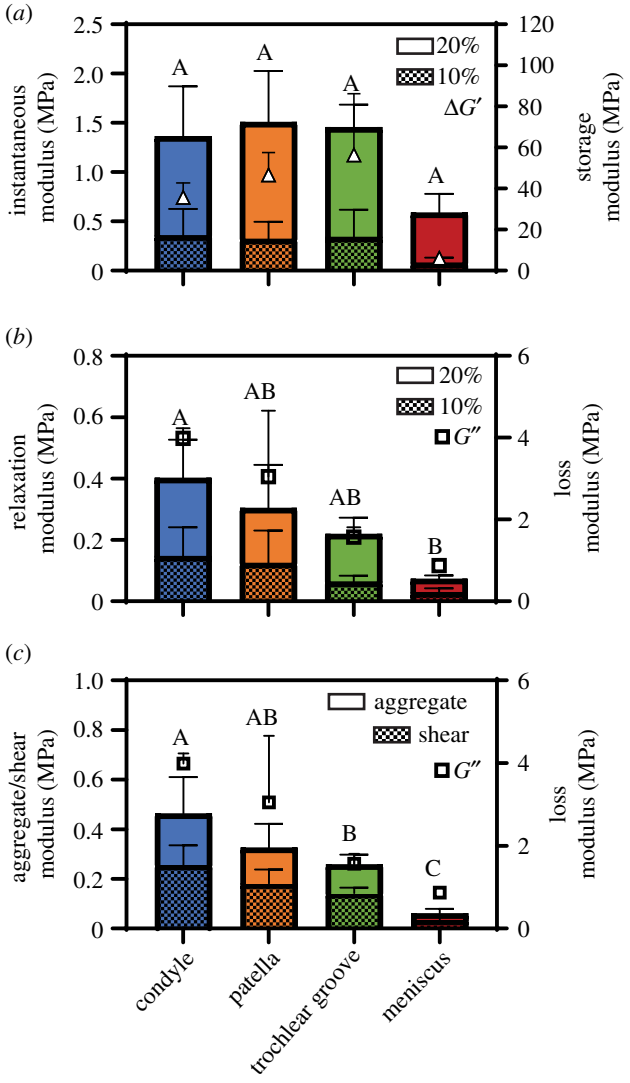

Figure 9. Quasi-static viscoelastic measurements with statistically significant correlations to dynamic measurements. Instantaneous (*a*) and relaxation (*b*) moduli from stress relaxation tests correlate to the storage (triangles) and loss (squares) moduli obtained from vibrometry, respectively. (*c*) Creep indentation tests show that both the aggregate and shear moduli also strongly correlate with the loss modulus. For simplicity, statistical differences shown here only pertain to the quasi-static measures (20% moduli for stress relaxation and aggregate modulus for creep indentation). Vibrometry values are only shown here as a reference. Error bars represent standard deviation and $n = 6$.

biochemical assays would elucidate cartilage's dynamic structure–function relationship. Lastly, the third hypothesis was that vibrometry would detect the differences in the dynamic mechanical properties among four regions of the knee, consisting of both hyaline and fibrocartilage. All three hypotheses were upheld. Vibrometry allowed for the measurement of phase shifts and calculation of storage and loss moduli, which correlated well with several standard quasi-static mechanical properties. Additionally, the loss moduli correlated strongly with GAG content, the tissue constituent that is typically related to compressive properties [41]. Moreover, dynamic properties not only differed among cartilage groups but also agreed with previously published work using non-vibrometry methods. These data show that the sole use of vibrometry can yield data obtained from three distinct assays. We found that vibrometry is an efficient and noncontact testing modality for native cartilage dynamic and viscoelastic testing and is well suited for providing necessary data in the regulatory process for knee cartilage replacement products.

This study showed that vibrometry is an important advancement towards noncontact dynamic mechanical testing of cartilage. Several strong correlations between traditional destructive assays used in cartilage research and dynamic mechanical properties obtained from noncontact vibrometry were found (figure 12). In this work, cartilage's viscoelasticity was described by the standard linear solid model, consisting of two elastic springs and a viscous dashpot (figure 3). Although the storage modulus (G') is associated with the relaxation modulus (equation (2.3*a*) and figure 3), it is also dependent on the spring-related 10% and 20% instantaneous moduli obtained from stress relaxation. Given the multiple relationships between G' and all of the standard linear solid's viscoelastic parameters, it was not surprising to find significant, albeit muted, correlations. With regard to biochemical components, there were no correlations with G'. The loss moduli (G''), associated with viscous behaviour, were correlated with measures from all the assays performed in this work. Previously described mathematical relationships between G'' and the mechanical components of the standard linear solid model imply that G'' should correlate with the Maxwell portion of the standard linear solid (figure 3) [26]. The present data's correlations between G'' and the 10% and 20% relaxation moduli were unexpected (statistical significance determined by $p = 0.052$ for 10% and $p = 0.031$ for 20%), given that the Maxwell spring depends on both the instantaneous and relaxation moduli ($E_1 = E_i - E_r$), but the single spring, E_2, is equivalent to the relaxation modulus. Since G'' only depends on E_1, its relationship may be related to other factors not contained within the standard linear solid's model. In this and other studies performed by

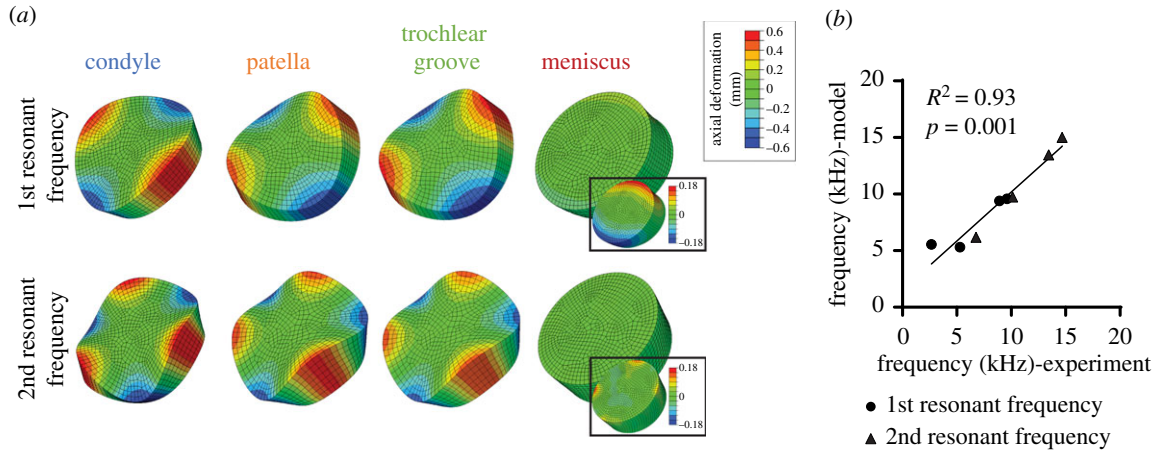

Figure 10. (*a*) Finite-element models predict resonant frequencies for each group based on input material properties. Predicted bending mode shapes resemble those observed experimentally. Meniscus deformations are small and autoscaled to observe the mode shapes (insets). (*b*) There is a strong correlation between experimental and modelled first (circles) and second (triangles) resonant frequencies ($R^2 = 0.93$).

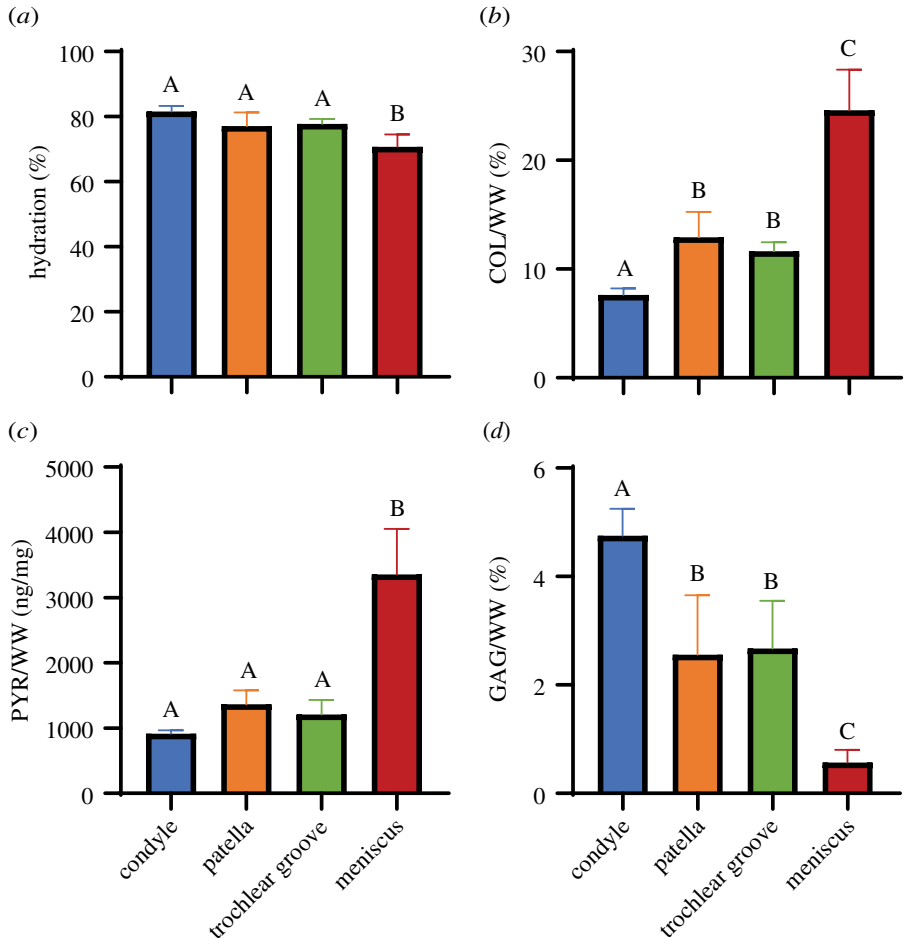

Figure 11. Biochemical composition differs across the cartilages of the knee. (*a*) Tissue hydration is relatively constant, with a slight, but significant decrease in meniscus samples. Collagen (*b*) and pyridinoline (*c*) content per wet weight (WW) are significantly higher in the meniscus compared to all other groups. (*d*) GAG content shows an inverse trend as compared to collagen and pyridinoline, with the condyle showing the highest percentages. Error bars represent standard deviation and $n = 6$.

our group, we have frequently found a similar relationship between the relaxation moduli from stress relaxation and aggregate moduli from creep experiments (data not shown). This is further reinforced by the correlations between G'' and the aggregate and shear moduli from creep indentation, as these are also measures of the long-term elastic response. It is possible that these surprising associations with G'' may be due to the high-frequency excitation used in our vibrometry experiments. It is well known that G' and G'' are frequency dependent and may even reach a 'crossover point' at which the relative relationship between these two moduli plateaus and is inverted [42,43]. This phenomenon has been observed in several biomaterials and tissues, such as collagen/hyaluronan gels [44], vocal fold tissue [45] and airway smooth muscle [46]. Therefore, although these particular relationships were not anticipated and merit further investigation, independent verification through both stress relaxation and creep indentation makes a very strong case for their validity.

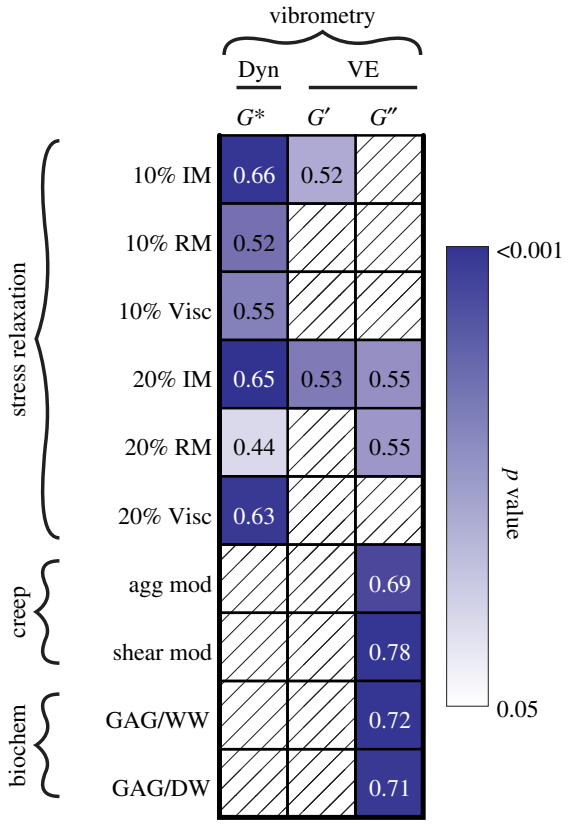

Figure 12. Strength and significance of Spearman ρ correlations between dynamic mechanical properties determined by vibrometry and quasi-static viscoelastic properties and biochemical content. Measurements are grouped together by curly brackets. With vibrometry, dynamic (Dyn) and viscoelastic (VE) properties can be obtained. IM, instantaneous modulus; RM, relaxation modulus; Visc, coefficient of viscosity; agg mod, aggregate modulus; and shear mod, shear modulus. Numbers indicate the strength of the correlation (ρ), and colour indicates the degree of significance. White boxes with diagonal lines denote that statistical significance was not achieved.

Notably, the correlations found in this study, especially between G'' and the creep-related parameters, suggest that quasi-static mechanical properties may predict dynamic properties. Inasmuch as the FDA and ASTM International recommend that both dynamic and viscoelastic properties be reported [8,47], these correlations demonstrate that vibrometry may obtain both dynamic and viscoelastic properties, an important observation in light of the regulatory requirements for cartilage tissue replacements.

Although biochemical composition is frequently used to describe cartilage's structure–function relationships, it is often only related to quasi-static mechanical measures. A few studies have investigated the association between cartilage composition and dynamic properties but typically only measure G^* without examining its elastic and viscous components [48,49]. In this study, the strongest correlations were found between the loss modulus (G'') and GAG content. This was not unexpected given the relationships between G'' and the relaxation, aggregate and shear moduli, described above. There were no correlations with collagen content. In the present work, the tissue was only axially perturbed. However, perturbations in different directions (e.g. parallel to the direction of articulation) may provide additional insights. A three-dimensional vibrometry set-up would detect radial and circumferential deformations, which would likely be correlated to collagen content. Further work to understand how dynamic mechanical properties relate to biochemical composition is needed, especially given the strong correlations reported in this study.

Vibrometer-based dynamic testing revealed differences in viscoelastic characteristics among the cartilage groups. G' (figure 7*b*) was similar to the dynamic modulus, G^* (figure 6*b*), for all groups. It has been previously reported that at high frequencies (greater than 40 Hz), cartilage behaves more like an elastic solid with reduced viscous contributions [1]. The small phase shifts (figure 7*a*) in the present study in which dynamic loading at 500 Hz (figure 2*c*) was employed support this, thus resulting in a relatively low G'' compared to the corresponding G' value (figure 7*c*). Phase shifts previously reported at 10 Hz [1] were comparable (approx. 5°) to our measured values, which averaged at 5.2°. However, despite these low phase shift values, there are significant differences in G'' among the groups. Interestingly, the meniscus, which is often described as a shock absorber, had the lowest G''. This is in contrast to condylar cartilage, which has the greatest G''. Values reported here are comparable to previously published data for both the condyle [50] and the meniscus [19]. Though the role of the meniscus as a shock absorber has been questioned [51,52], this is the first time that it has been quantitatively established that, using G'' as the outcome measure, condylar hyaline cartilage has a superior energy dissipation capacity when compared to the meniscus. Shock absorption has been quantified in numerous ways [53,54]; however, in this work, G'' was selected because it describes viscous energy dissipation independently from elastic energy storage. The vibrometer's ability to reproduce the viscoelastic properties of different knee cartilages is strongly demonstrated in this work and may continue to shed light onto the function of other types of cartilage in future studies.

The dynamic modulus of cartilage is the most basic measure of tissue function under the cyclic loading conditions found in daily locomotive activities. It should be noted that the dynamic moduli measured here (figure 6*b*) and reported elsewhere [1,20] are significantly greater (greater than 10×) than the moduli measured using quasi-static approaches (figure 9). This is due to internal fluid pressurization. Similar to quasi-static properties, there are topographical variations in dynamic properties across the different knee cartilages (figure 6). Here, an increasing trend was found from the condyle, patella, to trochlear groove groups; this has also been found by others in bovine tissues [20]. However, it is important to note that studies using human tissue report significantly greater compressive moduli for the condyle compared to the trochlear groove [55,56]. With regards to the meniscus, a separate study using human tissue [57] agreed with the meniscus data presented here. Both the data contained within the present study and independent studies [19,20,57] focusing on individual cartilages show that the meniscus has a lower dynamic compressive modulus when compared to values for the condyle, patella and trochlear groove. The compressive properties of the meniscus are known to be relatively small in comparison to its tensile properties, likely due to compressive load transfer into hoop stresses [19]. The hoop stresses are largely borne by the circumferential fibres found in the meniscus. This structural difference, as compared to the structure of hyaline cartilage, is likely responsible for the meniscus second mode shape and

expected given the literature on the effect of structure on the bending modes of composites [58–60]. Regardless of structure, the agreement in knee cartilage dynamic moduli obtained through noncontact vibrometry with previous reports using destructive methods is impressive and lends credence to vibrometry's efficacy.

Vibrometry's use for mechanical characterization of biological tissue is in its nascent stage, and thus requires further study and improvements to reach its potential. A limitation of this study is the use of high frequencies, beyond what is typically observed physiologically. This was required in our set-up in order to excite the entire specimen without damage. At low frequencies, vibrations merely resulted in translation, not the deformation or bending necessary to identify resonant frequencies. Although vibrometers can measure displacements at low frequencies, the mode of excitation would require increased contact, similar to what is used in destructive mechanical testing such as dynamic mechanical analysis (DMA). Therefore, it is expected that cartilage's viscoelastic properties would differ at lower frequencies typically used by other testing systems [61]. Despite this constraint, others have shown that cartilage's dynamic properties are relatively frequency stable when viscous properties are minimized at approximately 40 Hz and beyond [1,62–64]. This is supported by the similarity in G^* values reported here by resonant frequencies up to 15 kHz and those measured at 40 Hz [1]. Furthermore, our vibrometry-based storage and loss moduli measurements obtained for bovine hyaline articular cartilage at 15 kHz are within the same order of magnitude as those reported for human and bovine specimens using dynamic mechanical analysis at 88 Hz [62–64]. A related limitation to the translation of this work is the use of a piezoelectric drive to induce vibrations. The piezo did not damage the sample, thus allowing it to be used for other mechanical testing. However, *in situ* applications will require other means of vibrational excitation, such as ultrasound transducers [65]. A third limitation in this study may be that tissues remained in ambient conditions for the duration of the measurement. Although measurements were relatively short (less than 5 min), drying may be a concern. Given this concern, we have fabricated a fluid-filled sample chamber that nonetheless permits the piezo-mediated vibrations to excite the tissue and does not obstruct measurement. Preliminary data using this chamber (data not shown) are encouraging, yielding comparable results to those shown here and assuaging concerns regarding drying. It is important to note that vibrometry-based measurements for the entire study were completed in approximately 2 h, and provided information that collectively took 30 h to acquire from quasi-static mechanical tests and biochemical assays. This represents a 93% reduction in time. Lastly, we do not expect changes in tissue properties arising from enzymatic degradation or the freeze–thaw cycle in this work given that the joint remained closed prior to testing, cartilage cells are known to very metabolically inactive [66], and that refrigeration is the standard way of storing cartilage tissue [67]. However, this might not be the case when working with large samples, where properties can be affected by testing times; thus, groups working with large tissues and/or requiring a fast turnover will find this decrease in time of utmost importance. Given the benefits and advantages of vibrometry, optimization of this tool for cartilage research is well justified.

This study successfully shows the use of vibrometry in a noncontact manner to measure cartilage's dynamic mechanical properties. These properties were particularly distinctive to higher frequency dynamics, which may be representative of the high strain rates observed in traumatic injury. The dynamic properties reported here showed several correlations with quasi-static and biochemical properties, thus providing important insights into cartilage function under cyclic loading. Vibrometer-based measurements were also precise enough to detect differences in viscoelastic properties among the cartilages of the knee. This work not only solidifies the relationship among quasi-static, viscoelastic and dynamic properties over a short testing time but also presents a practical option for high-throughput nondestructive testing, ideal for applications in cartilage developmental biology, tissue engineering and translational medicine.

Data accessibility. Data available from the Dryad Digital Repository: https://doi.org/10.7280/D1WX12 [39]. Additional data are provided in the electronic supplementary material [68].

Authors' contributions. M.G.E.: Conceptualization, data curation, formal analysis, funding acquisition, investigation, methodology, project administration, validation, visualization, writing—original draft, writing—review and editing; G.A.O.: conceptualization, data curation, formal analysis, funding acquisition, investigation, methodology, writing—review and editing; J.C.H.: conceptualization, funding acquisition, methodology, project administration, supervision, writing—review and editing; K.A.A.: conceptualization, funding acquisition, project administration, resources, supervision, writing—review and editing.

All authors gave final approval for publication and agreed to be held accountable for the work performed therein.

Competing interests. We declare we have no competing interests.

Funding. The authors acknowledge support from the National Institutes of Health (grant nos R01 AR067821 and R01 AR071457), the National Institutes of Health Diversity Supplement (to M.G.E.), Fulbright Chile scholarship (to G.A.O.) and Becas Chile scholarship (to G.A.O.).

Acknowledgements. We thank Eric Lawrence, Jerome Eichenberger, Vicky Lu and Kilian Shambaugh from Polytec, Inc for their technical support.

References

1. Park S, Hung CT, Ateshian GA. 2004 Mechanical response of bovine articular cartilage under dynamic unconfined compression loading at physiological stress levels. *Osteoarthr. Cartil.* **12**, 65–73. (doi:10.1016/j.joca.2003.08.005)
2. Barker MK, Seedhom BB. 1997 Articular cartilage deformation under physiological cyclic loading—apparatus and measurement technique. *J. Biomech.* **30**, 377–381. (doi:10.1016/S0021-9290(96)00166-2)
3. Kaplan JT, Neu CP, Drissi H, Emery NC, Pierce DM. 2017 Cyclic loading of human articular cartilage: the transition from compaction to fatigue. *J. Mech. Behav. Biomed. Mater.* **65**, 734–742. (doi:10.1016/j.jmbbm.2016.09.040)
4. Zhang L, Miramini S, Smith DW, Gardiner BS, Grodzinsky AJ. 2015 Time evolution of deformation in a human cartilage under cyclic loading. *Ann. Biomed. Eng.* **43**, 1166–1177. (doi:10.1007/s10439-014-1164-8)
5. Bian L, Fong JV, Lima EG, Stoker AM, Ateshian GA, Cook JL, Hung CT. 2010 Dynamic mechanical loading enhances

functional properties of tissue-engineered cartilage using mature canine chondrocytes. *Tissue Eng. Part A.* **16**, 1781–1790. (doi:10.1089/ten.tea.2009.0482)

6. Krishnan R, Mariner EN, Ateshian GA. 2005 Effect of dynamic loading on the frictional response of bovine articular cartilage. *J. Biomech.* **38**, 1665–1673. (doi:10.1016/j.jbiomech.2004.07.025)
7. Mauck RL, Nicoll SB, Seyhan SL, Ateshian GA, Hung CT. 2003 Synergistic action of growth factors and dynamic loading for articular cartilage tissue engineering. *Tissue Eng.* **9**, 597–611. (doi:10.1089/107632703768247304)
8. Food and Drug Administration. 2011 *Preparation of IDEs and INDs for products intended to repair or replace knee cartilage*, pp. 1–18. Rockville, Maryland, USA: Center for Biologics Evaluation and Research.
9. Patel JM, Wise BC, Bonnevie ED, Mauck RL. 2019 A systematic review and guide to mechanical testing for articular cartilage tissue engineering. *Tissue Eng. C: Methods* **25**, 593–608. (doi:10.1089/ten.tec.2019.0116)
10. Olvera D, Daly A, Kelly DJ. 2015 Mechanical testing of cartilage constructs. In *Cartilage tissue engineering: methods and protocols* (ed. PM Doran), pp. 279–287. New York, NY: Springer New York.
11. Ronken S, Arnold M, Garcia HA, Jeger A, Daniels A, Wirz D. 2012 A comparison of healthy human and swine articular cartilage dynamic indentation mechanics. *Biomech. Model. Mechanobiol.* **11**, 631–639. (doi:10.1007/s10237-011-0338-7)
12. Rothberg SJ *et al.* 2017 An international review of laser Doppler vibrometry: making light work of vibration measurement. *Opt. Lasers Eng.* **99**, 11–22. (doi:10.1016/j.optlaseng.2016.10.023)
13. Dong W, Xia A, Raphael PD, Puria S, Applegate B, Oghalai JS. 2018 Organ of Corti vibration within the intact gerbil cochlea measured by volumetric optical coherence tomography and vibrometry. *J. Neurophysiol.* **120**, 2847–2857. (doi:10.1152/jn.00702.2017)
14. Wang X, Guan X, Pineda M, Gan RZ. 2016 Motion of tympanic membrane in guinea pig otitis media model measured by scanning laser Doppler vibrometry. *Hear. Res.* **339**, 184–194. (doi:10.1016/j.heares.2016.07.015)
15. Corbin EA, Adeniba OO, Ewoldt RH, Bashir R. 2016 Dynamic mechanical measurement of the viscoelasticity of single adherent cells. *Appl. Phys. Lett.* **108**, 093701. (doi:10.1063/1.4942364)
16. Desjardins CL, Antonelli LT, Soares E. 2007 *A remote and non-contact method for obtaining the blood-pulse waveform with a laser Doppler vibrometer. Advanced biomedical and clinical diagnostic systems V.* In *Proc. SPIE 6430, Advanced Biomedical and Clinical Diagnostic Systems V, 6 February 2007,* 64301C. (doi:10.1117/12.701139)
17. Zhang X, Kinnick R, Pittelkow M, Greenleaf JF (eds). 2008 Skin viscoelasticity with surface wave method. In *2008 IEEE Ultrasonics Symp, Beijing, China, 2–5 November 2008*, pp. 651–653. Piscataway, NJ: Institute of Electrical and Electronics Engineers.
18. Schwarz S, Hartmann B, Sauer J, Burgkart R, Sudhop S, Rixen D, Clausen-Schaumann H. 2020 Contactless vibrational analysis of transparent hydrogel structures using laser-Doppler vibrometry. *Exp. Mech.* **60**, 1067–1078. (doi:10.1007/s11340-020-00626-0)
19. Danso E, Mäkelä J, Tanska P, Mononen M, Honkanen J, Jurvelin J, Töyräs J, Julkunen P, Korhonen RK. 2015 Characterization of site-specific biomechanical properties of human meniscus—importance of collagen and fluid on mechanical nonlinearities. *J. Biomech.* **48**, 1499–1507. (doi:10.1016/j.jbiomech.2015.01.048)
20. Laasanen M, Töyräs J, Korhonen R, Rieppo J, Saarakkala S, Nieminen M, Hirvonen J, Jurvelin JS. 2003 Biomechanical properties of knee articular cartilage. *Biorheology.* **40**, 133–140.
21. Richler D, Rittel D. 2014 On the testing of the dynamic mechanical properties of soft gelatins. *Exp. Mech.* **54**, 805–815. (doi:10.1007/s11340-014-9848-4)
22. Rotbaum Y, Puiu C, Rittel D, Domingos M. 2019 Quasi-static and dynamic *in vitro* mechanical response of 3D printed scaffolds with tailored pore size and architectures. *Mater. Sci. Eng.: C.* **96**, 176–182. (doi:10.1016/j.msec.2018.11.019)
23. Jurvelin JS, Arokoski JPA, Hunziker EB, Helminen HJ. 2000 Topographical variation of the elastic properties of articular cartilage in the canine knee. *J. Biomech.* **33**, 669–675. (doi:10.1016/S0021-9290(00)00007-5)
24. ATSM International. 2001 *Standard test method for dynamic Young's modulus, shear modulus, and Poisson's ratio by impulse excitation of vibration*. West Conshohocken, PA: ASTM International.
25. Martinček G. 1965 The determination of Poisson's ratio and the dynamic modulus of elasticity from the frequencies of natural vibration in thick circular plates. *J. Sound Vib.* **2**, 116–127. (doi:10.1016/0022-460X(65)90089-1)
26. Athanasiou KA, Natoli RM. 2008 Introduction to continuum biomechanics. *Synth. Lect. Biomed. Eng.* **3**, 1–206. (doi:10.2200/S00121ED1V01Y200805BME019)
27. Allen KD, Athanasiou KA. 2006 Viscoelastic characterization of the porcine temporomandibular joint disc under unconfined compression. *J. Biomech.* **39**, 312–322. (doi:10.1016/j.jbiomech.2004.11.012)
28. Athanasiou K, Agarwal A, Dzida F. 1994 Comparative study of the intrinsic mechanical properties of the human acetabular and femoral head cartilage. *J. Orthop. Res.* **12**, 340–349. (doi:10.1002/jor.1100120306)
29. Athanasiou K, Niederauer G, Schenck R. 1995 Biomechanical topography of human ankle cartilage. *Ann. Biomed. Eng.* **23**, 697–704. (doi:10.1007/BF02584467)
30. Mow VC, Kuei S, Lai WM, Armstrong CG. 1980 Biphasic creep and stress relaxation of articular cartilage in compression: theory and experiments. *J. Biomech. Eng.* **102**, 73–84. (doi:10.1115/1.3138202)
31. Mow VC, Gibbs MC, Lai WM, Zhu WB, Athanasiou KA. 1989 Biphasic indentation of articular cartilage—II. A numerical algorithm and an experimental study. *J. Biomech.* **22**, 853–861. (doi:10.1016/0021-9290(89)90069-9)
32. Athanasiou K, Agarwal A, Muffoletto A, Dzida F, Constantinides G, Clem M. 1995 Biomechanical properties of hip cartilage in experimental animal models. *Clin. Orthop. Relat. Res.* **316**, 254–266. (doi:10.1097/00003086-199507000-00035)
33. Ateshian G, Lai W, Zhu W, Mow V. 1994 An asymptotic solution for the contact of two biphasic cartilage layers. *J. Biomech.* **27**, 1347–1360. (doi:10.1016/0021-9290(94)90044-2)
34. Lilledahl MB, Pierce DM, Ricken T, Holzapfel GA, de Lange Davies C. 2011 Structural analysis of articular cartilage using multiphoton microscopy: input for biomechanical modeling. *IEEE Trans. Med. Imaging.* **30**, 1635–1648. (doi:10.1109/TMI.2011.2139222)
35. Ferguson S, Bryant J, Ganz R, Ito K. 2000 The influence of the acetabular labrum on hip joint cartilage consolidation: a poroelastic finite element model. *J. Biomech.* **33**, 953–960. (doi:10.1016/S0021-9290(00)00042-7)
36. Cissell DD, Link JM, Hu JC, Athanasiou KA. 2017 A modified hydroxyproline assay based on hydrochloric acid in Ehrlich's solution accurately measures tissue collagen content. *Tissue Eng. C: Methods* **23**, 243–250. (doi:10.1089/ten.tec.2017.0018)
37. Gonzalez-Leon EA, Bielajew BJ, Hu JC, Athanasiou KA. 2020 Engineering self-assembled neomenisci through combination of matrix augmentation and directional remodeling. *Acta Biomater.* **109**, 73–81. (doi:10.1016/j.actbio.2020.04.019)
38. Schober P, Boer C, Schwarte LA. 2018 Correlation coefficients: appropriate use and interpretation. *Anesth. Analg.* **126**, 1763–1768. (doi:10.1213/ANE.0000000000002864)
39. Espinosa MG, Otarola GA, Hu JC, Athanasiou K. 2021 Dataset for vibrometry as a noncontact alternative to dynamic and viscoelastic mechanical testing in cartilage. Dryad Digital Repository (doi:10.7280/D1WX12)
40. Thompson D. 2008 Railway noise and vibration: mechanisms, modelling and means of control. Oxford, UK: Jordan Hill.
41. Kim Y-J, Grodzinsky AJ, Plaas AH. 1996 Compression of cartilage results in differential effects on biosynthetic pathways for aggrecan, link protein, and hyaluronan. *Arch. Biochem. Biophys.* **328**, 331–340. (doi:10.1006/abbi.1996.0181)
42. Mason TG, Weitz DA. 1995 Optical measurements of frequency-dependent linear viscoelastic moduli of complex fluids. *Phys. Rev. Lett.* **74**, 1250. (doi:10.1103/PhysRevLett.74.1250)
43. Winter HH. 1987 Can the gel point of a cross-linking polymer be detected by the G′–G″crossover? *Polym. Eng. Sci.* **27**, 1698–1702. (doi:10.1002/pen.760272209)
44. Yang Y-I, Kaufman LJ. 2009 Rheology and confocal reflectance microscopy as probes of mechanical

properties and structure during collagen and collagen/hyaluronan self-assembly. *Biophys. J.* **96**, 1566–1585. (doi:10.1016/j.bpj.2008.10.063)

45. Chan RW, Rodriguez ML. 2008 A simple-shear rheometer for linear viscoelastic characterization of vocal fold tissues at phonatory frequencies. *J. Acoust. Soc. Am.* **124**, 1207–1219. (doi:10.1121/1.2946715)
46. Ito S, Majumdar A, Kume H, Shimokata K, Naruse K, Lutchen KR, Stamenovic D, Suki B. 2006 Viscoelastic and dynamic nonlinear properties of airway smooth muscle tissue: roles of mechanical force and the cytoskeleton. *Am. J. Physiol.-Lung Cell. Mol. Physiol.* **290**, L1227–L1237. (doi:10.1152/ajplung.00299.2005)
47. ASTM International. 2005 *Standard guide for in vivo assessment of implantable devices intended to repair or regenerate articular cartilage*. West Conshohocken, PA: ASTM International.
48. Burgin LV, Edelsten L, Aspden RM. 2014 The mechanical and material properties of elderly human articular cartilage subject to impact and slow loading. *Med. Eng. Phys.* **36**, 226–232. (doi:10.1016/j.medengphy.2013.11.002)
49. Gannon AR, Nagel T, Kelly DJ. 2012 The role of the superficial region in determining the dynamic properties of articular cartilage. *Osteoarthr. Cartil.* **20**, 1417–1425. (doi:10.1016/j.joca.2012.08.005)
50. Fulcher GR, Hukins DWL, Shepherd DET. 2009 Viscoelastic properties of bovine articular cartilage attached to subchondral bone at high frequencies. *BMC Musculoskelet. Disord.* **10**, 61. (doi:10.1186/1471-2474-10-61)
51. Andrews S, Shrive N, Ronsky J. 2011 The shocking truth about meniscus. *J. Biomech.* **44**, 2737–2740. (doi:10.1016/j.jbiomech.2011.08.026)
52. Gaugler M, Wirz D, Ronken S, Hafner M, Göpfert B, Friederich NF, Elke R. 2015 Fibrous cartilage of human menisci is less shock-absorbing and energy-dissipating than hyaline cartilage. *Knee Surg. Sports Traumatol. Arthrosc.* **23**, 1141–1146. (doi:10.1007/s00167-014-2926-4)
53. Dahl MC, Jacobsen S, Metcalf Jr N, Sasso R, Ching RP. 2011 A comparison of the shock-absorbing properties of cervical disc prosthesis bearing materials. *SAS J.* **5**, 48–54. (doi:10.1016/j.esas.2011.01.002)
54. Dura JV, Garcia AC, Solaz J. 2002 Testing shock absorbing materials: the application of viscoelastic linear model. *Sports Eng.* **5**, 9–14. (doi:10.1046/j.1460-2687.2002.00085.x)
55. Lyyra T, Kiviranta I, Väätäinen U, Helminen HJ, Jurvelin JS. 1999 In vivo characterization of indentation stiffness of articular cartilage in the normal human knee. *J. Biomed. Mater. Res.* **48**, 482–487. (doi:10.1002/(SICI)1097-4636(1999)48:4<482::AID-JBM13>3.0.CO;2-M)
56. Shepherd D, Seedhom B. 1999 The 'instantaneous' compressive modulus of human articular cartilage in joints of the lower limb. *Rheumatology (Oxford)* **38**, 124–132. (doi:10.1093/rheumatology/38.2.124)
57. Chia HN, Hull M. 2008 Compressive moduli of the human medial meniscus in the axial and radial directions at equilibrium and at a physiological strain rate. *J. Orthop. Res.* **26**, 951–956. (doi:10.1002/jor.20573)
58. Hou JP, Jeronimidis G. 2000 Bending stiffness of composite plates with delamination. *Compos. A: Appl. Sci. Manuf.* **31**, 121–132. (doi:10.1016/S1359-835X(99)00064-0)
59. Lv N, Zhong C, Wang L. 2021 Bending vibration characteristics of the piezoelectric composite double laminated vibrator. *Ceram. Int.* **47**, 31 259–31 267. (doi:10.1016/j.ceramint.2021.07.302)
60. Oh K, Nayfeh AH. 1996 Nonlinear combination resonances in cantilever composite plates. *Nonlinear Dyn.* **11**, 143–169. (doi:10.1007/BF00044999)
61. Cacopardo L, Mattei G, Ahluwalia A. 2020 A new load-controlled testing method for viscoelastic characterisation through stress-rate measurements. *Materialia* **9**, 100552. (doi:10.1016/j.mtla.2019.100552)
62. Cooke ME, Lawless BM, Jones SW, Grover LM. 2018 Matrix degradation in osteoarthritis primes the superficial region of cartilage for mechanical damage. *Acta Biomater.* **78**, 320–328. (doi:10.1016/j.actbio.2018.07.037)
63. Lawless BM, Sadeghi H, Temple DK, Dhaliwal H, Espino DM, Hukins DW. 2017 Viscoelasticity of articular cartilage: analysing the effect of induced stress and the restraint of bone in a dynamic environment. *J. Mech. Behav. Biomed. Mater.* **75**, 293–301. (doi:10.1016/j.jmbbm.2017.07.040)
64. Temple DK, Cederlund AA, Lawless BM, Aspden RM, Espino DM. 2016 Viscoelastic properties of human and bovine articular cartilage: a comparison of frequency-dependent trends. *BMC Musculoskelet. Disord.* **17**, 1–8. (doi:10.1186/s12891-016-1279-1)
65. Castro NJ, Babakhanova G, Hu J, Athanasiou KA. 2021 Nondestructive testing of native and tissue-engineered medical products: adding numbers to pictures. *Trends Biotechnol.* (doi:10.1016/j.tibtech.2021.06.009)
66. Das R, Van Osch G, Kreukniet M, Oostra J, Weinans H, Jahr H. 2010 Effects of individual control of pH and hypoxia in chondrocyte culture. *J. Orthop. Res.* **28**, 537–545. (doi:10.1002/jor.20994)
67. Espinosa MG, Otarola GA, Hu JC, Athanasiou KA. 2021 Cartilage assessment requires a surface characterization protocol: roughness, friction, and function. *Tissue Eng. C: Methods* **27**, 276–286. (doi:10.1089/ten.tec.2020.0367)
68. Espinosa MG, Otarola GA, Hu JC, Athanasiou K. 2021 Vibrometry as a noncontact alternative to dynamic and viscoelastic mechanical testing in cartilage. Figshare.